Soft Matter

Dynamics and rheology of nonpolar bijels

Journal:	*Soft Matter*
Manuscript ID:	SM-ART-04-2015-000994.R1
Article Type:	Paper
Date Submitted by the Author:	31-May-2015

Complete List of Authors:	Bai, Lian; University of Minneasota, Chemical Engineering and Materials Science; Univerisity of Minnesota, Chemical Engineering and Materials Science; Lian Bai, Fruehwirth, John; Univerisity of Minnesota, Chemical Engineering and Materials Science Cheng, Xiang; Univerisity of Minnesota, Chemical Engineering and Materials Science Macosko, Christopher; Univerisity of Minnesota, Chemical Engineering and Materials Science

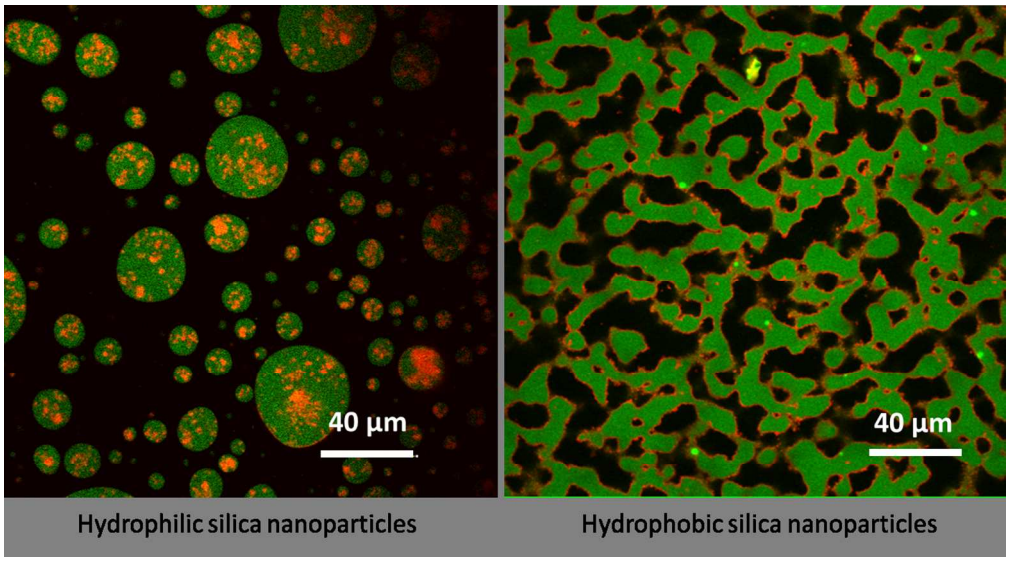

Confocal images of PS/PB/P-SNP droplet-martix blend (left) and PS/PB/B-SNP bijel (right)

Dynamics and rheology of nonpolar bijels

Lian Bai, John W. Fruehwirth, Xiang Cheng*, Christopher W. Macosko*

Department of Chemical Engineering and Materials Science, University of Minnesota, Minneapolis, Minnesota, 55455, USA

Abstract

Bicontinuous, interfacially jammed, emulsion gels (bijels) are a novel class of materials composed of two immiscible phases with interpenetrating domains that are stabilized by a monolayer of colloidal particles at the interface. However, existing bijel systems so far all consist of at least one polar fluid, which is believed to be essential to induce electrostatic repulsion for stabilizing interfacial particles. It is not known whether two nonpolar fluids can form a bijel. Here, we experimentally achieve a bijel using styrene trimers and low molecular weight polybutene—two nonpolar fluids that are similar to polymer blends, which are important in technical applications. By combining laser scanning confocal microscopy, cryo-SEM and rheology measurement, we systematically investigate the dynamics and rheology of this nonpolar bijel. In contrast to previous studies on polar bijels, we observe the formation of localized regions of high particle concentration or "particle patches" on the interface which assemble during coarsening. We also provide the first quantitative relation between the morphology of a bijel, the interfacial particle coverage and the shear modulus during bijel coarsening. Moreover, we reveal a previously unnoticed increase in the elastic modulus of bijels that can be attributed to the rearrangement of interfacial particles at long time scales. In addition, we also found a hydrophobic particle framework that survives after the direct remixing of the nonpolar bijel. Our study provides important insights into the formation of bijels and is the first step to explore the missing link between polar bijels and particle-stabilized polymer bicontinuous blends.

1. Introduction

Bicontinuous, interfacially jammed, emulsion gels (bijels) are a new class of soft materials that are composed of two interpenetrating low-viscosity fluids. The bicontinuous morphology is stabilized by a monolayer of particles jammed at the interface through spinodal decomposition[1,2]. Bicontinuous structures impart superior transport and mechanical properties and can be used in many technological applications including scaffolds in tissue engineering[3,4], cross-flow microreactors in chemical engineering[5] and electrochemical devices[6]. Given their importance, it is not surprising that there is growing interest in bicontinuous structures.

To date, only two bijel compositions have been experimentally realized, i.e., water/2,6-lutidine (W/L)[5,7] and nitromethane/ethylene glycol (NM/EG)[8,9]. Both these bijels are polar systems, which have at least one strongly polar fluid to induce electrostatic repulsion (Coulomb or dipole-dipole interaction) to balance the attraction from capillary forces[10,11,12] between neighboring particles at the interface[13,14]. It is still unknown whether particles can fully cover and jam the interface between two *nonpolar* fluids and thus lead to nonpolar bijels. For example, Cheng and Velankar[15] found that iron oxide particles spread easily on polar ethylene glycol/mineral oil interfaces but formed patches, regions of high particle concentration, on a nonpolar mineral oil/silicone oil interface due to the lack of electrostatic repulsion. On the other hand, Vermant and co-workers[16,17] found that hydrophobic silica nanoparticles accumulate on the nonpolar interface of a polyisobutylene (PIB)/polydimethylsiloxane (PDMS) drop-matrix blend and effectively suppress the coalescence of PIB droplets, although it is not clear from their experiments whether the particles form a monolayer on the interface. To the best of our knowledge, none of experiments so far has been able to successfully achieve bijels with two nonpolar fluids. Moreover, although the morphology and rheology of bijels during coarsening have been documented separately[9,18], there still lacks a systematic study to quantitatively correlate the dynamics of structural change, the degree of

interfacial particle coverage and the rheological variation during the formation of bijels.

Here, we used the hydrophobic silica nanoparticles (B-SNP) to stabilize the bicontinuous structure of styrene trimers (PS) and low molecular weight polybutenes (PB) and thus experimentally realized the first nonpolar bijel. The polarities of materials in this and previous studies are compared in Fig. 1. Combining laser-scanning confocal microscopy, cryogenic scanning electron microscopy and rheological measurements, we investigated the change of bijel morphology as well as the variation of interfacial particle coverage and rheology during coarsening. By analyzing and correlating the time scales extracted from these three dynamical measurements, we integrated a comprehensive picture of how particles suppress the coarsening and stabilize the morphology in bijels. We also found the formation of particle patches on the interface which grew larger during the coarsening in our nonpolar bijels. Such patches are not expected to occur in polar bijels. In addition, we uncovered a new rheological feature of particle-stabilized bicontinuous structures which occurs in both polar[18] and nonpolar bijels and in conventional immiscible polymer blends[19]: the continuous increase of storage modulus long after the stabilization of bicontinuous morphology. We also found that the particle framework formed at the interface maintains even after the PS/PB phases are re-mixed. Although this so-called "monogel" structure has been reported in polar bijels[18,20], we argue that the formation of a particle framework in nonpolar bijels arises from the nonpolar nature of particle-matrix and inter-particle interactions.

Finally, it is worth noting that compared with polar bijels, the styrene trimers and polybutenes in our bijel are more directly relevant to polymer components in particle-stabilized bicontinuous polymer blends[19,21,22,23,24], which share similar polarities and chemical structures. Thanks to the low viscosity of the PS/PB/B-SNP bijel (~10-10^2 Pa·s at room temperature) and the fluorescent B-SNP, we are able to directly image the real-time dynamics of the coarsening of bicontinuous structure that has not been possible in any other related particle-stabilized polymer systems[21,22,23,24].

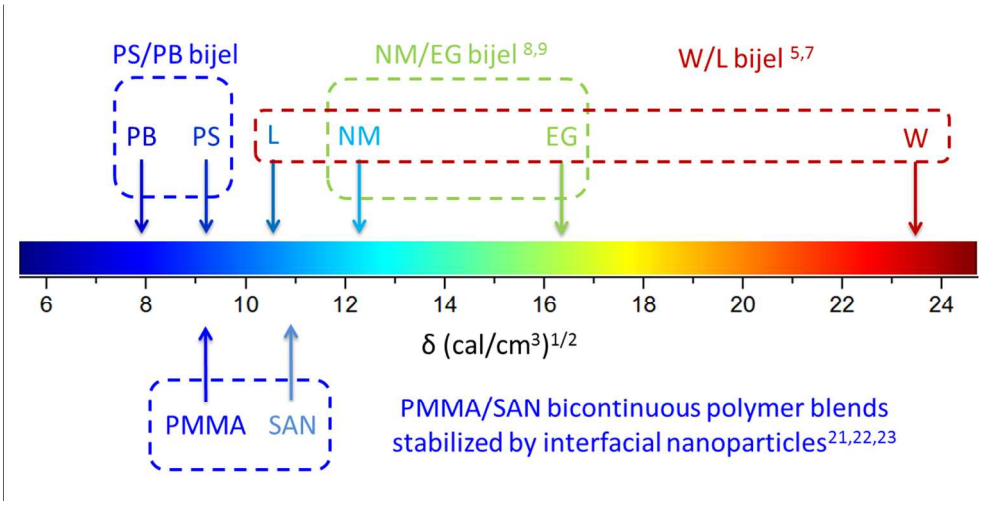

Fig. 1 Comparison of polarities in different bicontinuous systems. The polarities of materials are quantified by the solubility parameter, δ. The values of δ are: water (W, 23.4), 2,6-ludine (L, 10.6), nitromethane (NM, 12.3), ethylene glycol (EG, 16.3), styrene trimers (PS, ~9.2), polybutene (PB, 7.9), poly(methyl methacrylate) (PMMA, 9.2) and poly(styrene-*co*-acrylonitrile) (SAN, ~10.9). [25,26]

2. Materials and methods

2.1 Materials and particle synthesis

Low molecular weight hydrocarbon resin composed of styrene trimer (PS, Piccolastic A5 Hydrocarbon Resin, M_n = 300, PDI = 1.2, Eastman) and polybutene (PB, PB-24, M_n = 950, Soltex) were used as received. Physical properties of these two nonpolar materials and the synthesized silica nanoparticles (SNP) are listed in Table 1.

Table 1 Material properties

Materials	Viscosity at 25 °C (η_∞, Pa s)	Density (ρ, g/cm^3)	Refractive index, n(20/D)
PS-A5	33.4	0.96	1.52 ~ 1.55
PB-24	24.1	0.89	~ 1.49
SNP	NA	2.2	~ 1.544

We used the well-known Stober method to synthesize monodisperse fluorescent hydrophilic silica nanoparticles (P-SNP).[27,28] Before synthesis, fluorescent cores were prepared by addition of 28 mg of rhodamine B isothiocyanate (RITC, Sigma-Aldrich) to

a solution of 5 mL anhydrous ethanol and 44 mg 3-aminopropyltriethoxysilane (APTES, Sigma-Aldrich). The dye solution was then stirred overnight in a 25 mL round-bottom flask at room temperature. The particles were synthesized by adding 7.7 mL ammonia (29% w/w, Sigma-Aldrich), 4.6 mL DI water, 7.7 mL tetraethylorthosilicate (TEOS, > 99%, Sigma-Aldrich) and 5 mL fluorescent core suspension to 176 mL of anhydrous ethanol, and stirring the reaction for 6 hr in a 500 mL round-bottom flask at room temperature. Particle size distribution was characterized by dynamic light scattering (DLS, Brookhaven Instruments Corp. NanoBrook 90Plus Zeta Particle Size Analyzer): the hydrodynamic diameter = 102 nm ± 4 nm. Scanning electron microscopy (SEM, JEOL 6500F) was also used, which confirmed the diameter of the dry particles at ~100 nm.

Hydrophobic modification of the fluorescent P-SNP was achieved via hexamethyldisilazane (HMDS, 98%, Alfa Aesar).[8,9] An appropriate amount of HMDS was directly added to the reaction mixture of the synthesized P-SNP. The mixture was stirred for 5 days to accomplish the silanization reaction. The fluorescent hydrophobic silica nanoparticles (B-SNP) were subsequently washed twice with ethanol to remove unreacted chemicals and excess fluorescent dye. Finally, the B-SNP was dispersed in tetrahydrofuran (THF) via ultrasonic bath for 10 min before further use during preparation of PS/PB/B-SNP bijels.

2.2 Cloud point test

A phase diagram of the PS/PB blend was constructed by measuring transmitted light intensity as a function of temperature.[29,30] Samples were loaded in a 1 mL ampoule located in a hole of an aluminum heat stage, allowed to equilibrate in the one-phase region above the UCST of the PS/PB blends and then were cooled to room temperature at a rate of ~ 0.4^{o}C/min. We determined the cloud point when the transmitted light intensity decreased to nearly zero (Fig. 2 inset).

Fig. 2 displays the cloud point curve of neat blend with different weight fractions of

PS. Due to kinetic effects, the cloud point is usually located between the binodal and spinodal line.[31] Nevertheless, the cloud point curve reflects the basic phase behavior of the PS/PB blends used in this study (dash line in Fig. 2): UCST locates at ~ 50 ^{o}C for 80 wt% PS. Hence, for PS/PB neat blends (50/50 wt%) and the corresponding PS/PB/B-SNP bijels, only a deep rapid quench can safely suppress the nucleation-growth of the immiscible phase in the metastable region and move the sample into the unstable region under the spinodal line, where bicontinuous morphology can be formed via spinodal decomposition.[32]

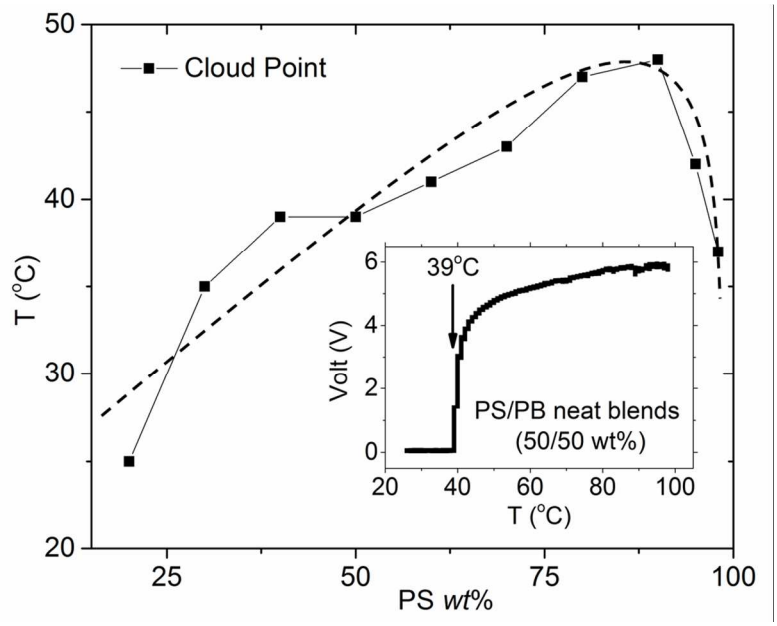

Fig. 2 Cloud point curve of PS/PB neat blend with different PS composition. The dashed line was drawn to guide the eye. The inset illustrates determination of the cloud point for a 50/50 wt% neat blend. Transmitted light intensity (photocell voltage) is plotted as a function of temperature.

2.3 Blends preparation

Equal amounts of PS and PB were dissolved in a suspension of B-SNP in THF. The mixture was dried in an oven at 80 ^{o}C for 24 hr to remove the THF. The PS/PB/SNP blend were denoted by (*A*/*B*/*x*), where *A* and *B* represent the weight fraction of PS and PB in the binary blend, respectively, and *x* is the weight fraction of SNP with respect to the total amount of PS/PB matrix. In this study, x = 0.5, 2.0 and 4.5 were used. Since the

UCST-type phase-separation temperature is ~ 40 ^{o}C for PS/PB (50/50 wt%) blend (Fig. 2), the resulting PS/PB/SNP blend are homogenous at 80 ^{o}C. The PS/PB/SNP (50/50/*x*) blend was transferred to a sample cell (Fig. 3a) which was preheated to 80 ^{o}C. The cell was quenched below the phase-separation temperature by placing it between dry ice blocks (-78 ^{o}C) causing the bicontinuous morphology to form through spinodal decomposition.

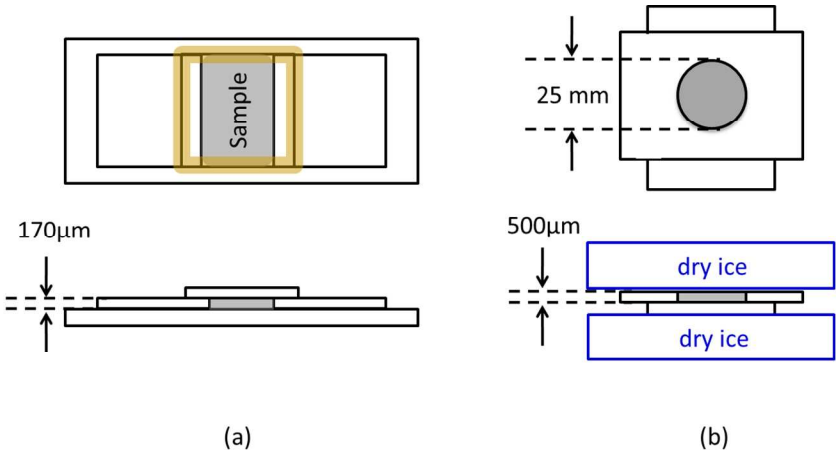

Fig. 3 (a) Top view and cross section of the confocal sample cell: a bottom glass side serves as the holder, two pieces of cover glass in the middle as spacers and a cover glass on the top for microscope observation. Epoxy (yellow) was used to glue the cover glasses on the bottom slide. The sample is contained in the gray region. (b) Top view and cross section of the mold for preparing PS/PB/B-SNP blend for rheological measurements: a bottom stainless steel plate topped with another stainless steel plate with a central hole 25 mm in diameter. The sample is placed inside the hole (gray area). Dry ice in a sandwich structure is used to quench the sample into a bicontinuous morphology.

2.4 Confocal microscopy

We used laser scanning confocal microscopy (LSCM, Olympus Fluo View 1000) to study the dynamics of the PS/PB/B-SNP bijels. Unless explicitly stated, the images were always taken at room temperature (20 ^{o}C).

The refractive index difference between PS, PB and SNP is small enough to allow us to image the sample ~30 μm below the coverslip. We used two different laser channels for imaging. Picolastic PS in this study was fluorescent when excited by a 488 nm laser beam, allowing the two phases to be distinguished in the first channel (green region in Fig. 4). A second, 563 nm laser was used to excite the RITC dye in the SNP, allowing

detection of SNP through the second channel (red dots in Fig. 4). Note that due to the small size of the particles, we cannot identify individual SNP in our images. The locations of particles were determined within ~ 200 nm, a limit set by the diffraction of light.

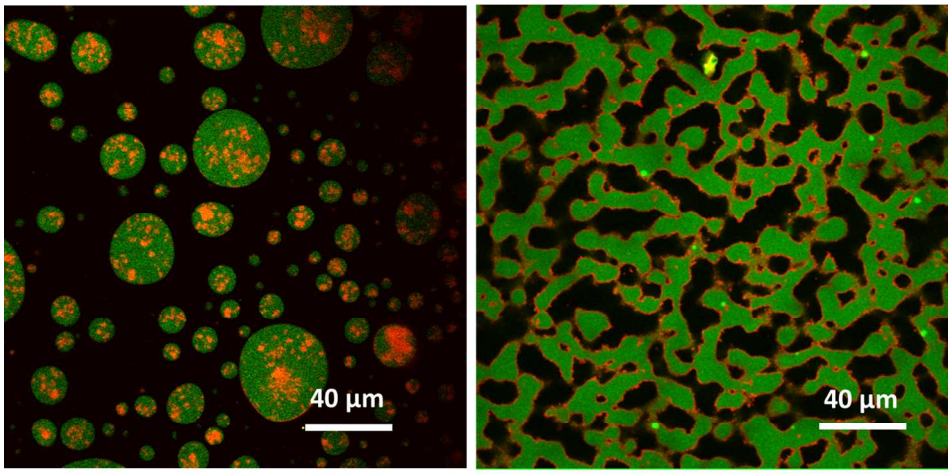

Fig. 4 Confocal images of (a) PS/PB/P-SNP (50/50/4.5) droplet-matrix blend; (b) PS/PB/B-SNP (50/50/4.5) bijel. The green region is PS, black region is PB and the red dots represent particles.

To analyze the change of domain size during coarsening, we thresholded the confocal images to create binary images. The interface length, L_{int}, was then obtained by tracking the interface between the black and white regions in the binary images. The characteristic domain size (ξ) can thus be defined as $1/Q$, where Q is the interfacial length per unit area, $Q = L_{int}/S$ and S is the total area of the confocal image.

Similar binary images can also been obtained from the second channel with the 563 nm laser. The location of SNP can be estimated using this channel. We combined the confocal images from these two channels to analyze the degree of interfacial coverage by nanoparticles. In this analysis, we directly compared the position of the PS/PB interface from the first channel with the position of nanoparticles from the second channel. Interfacial coverage is defined as the fraction of the PS/PB interface that is occupied by nanoparticles. Due to the pixel noise of imaging, the following criterion was adopted to determine coverage: the PS/PB interface from the first channel is covered by particles

only if the corresponding pixel or one of the eight nearest neighboring pixels around the corresponding pixel from the second channel is occupied by particles.

2.5 Cryogenic scanning electron microscopy

We also used cryogenic scanning electron microscopy (cryo-SEM) to visualize the location of B-SNP. Cryo-SEM images were taken using a Hitachi SU8320 field emission gun scanning electron microscope with Leica Cryostage. The PS/PB/B-SNP bijel was first placed in a small capillary, which was then quenched in liquid nitrogen. Afterwards, we transferred the capillary to a preparation chamber (-160 ^{o}C), where the sample was fractured then coated with a thin platinum layer. Finally, the sample was transferred to the cryo-SEM chamber (-130 ^{o}C) under high vacuum for SEM imaging.

2.6 Rheological characterization

Rheological measurements of the PS/PB neat blend and the PS/PB/B-SNP bijels were performed on a rotational rheometer (AR-G2, TA Instruments) with a Peltier temperature control stage as the bottom plate. We used the parallel plate geometry with a diameter of 25 mm and a gap height of 400 μm. PS/PB/B-SNP bijels was formed by quenching from 80 ^{o}C to -78 ºC in a sandwich structure by dry ice blocks (Fig. 3b). Afterwards, we removed the spacer and transferred the disk-shaped sample on the plate holder to the Peltier stage (0 ^{o}C) of the rheometer. After setting the gap and stabilizing the plate holder on the stage with thermally conductive tape, the sample was heated back to room temperature (20 ^{o}C) to take a dynamic time sweep at 0.1% strain and 1 rad/s. Frequency sweeps were also performed from 0.02 to 100 rad/s.

3. Results and discussion

3.1 Formation and microstructure of PS/PB/B-SNP bijels

Even though bicontinuous morphology can be achieved for the neat PS/PB blends

via spinodal decomposition by a deep quench, the bicontinuous structure quickly coalesces and collapses to droplet-matrix morphology. To stabilize the bicontinuous morphology, we tested silica nanoparticles with different wetting properties. For hydrophilic silica nanoparticles (P-SNP), the PS/PB/P-SNP (50/50/4.5) blend gave droplet-matrix morphology (Fig. 4a). The particles aggregated in the PS phase. In contrast, bicontinuous morphology was achieved when the hydrophobic silica nanoparticles (B-SNP) were used (Fig. 4b and Supplementary Information, Video SV1). The cryo-SEM images in Fig. 5 show that the particles are located at the interface between the two phases and form monolayers. These images look similar to those of Virgilio *et al* for a three component polymer blend where the minor phase formed droplets at the interface.[36]

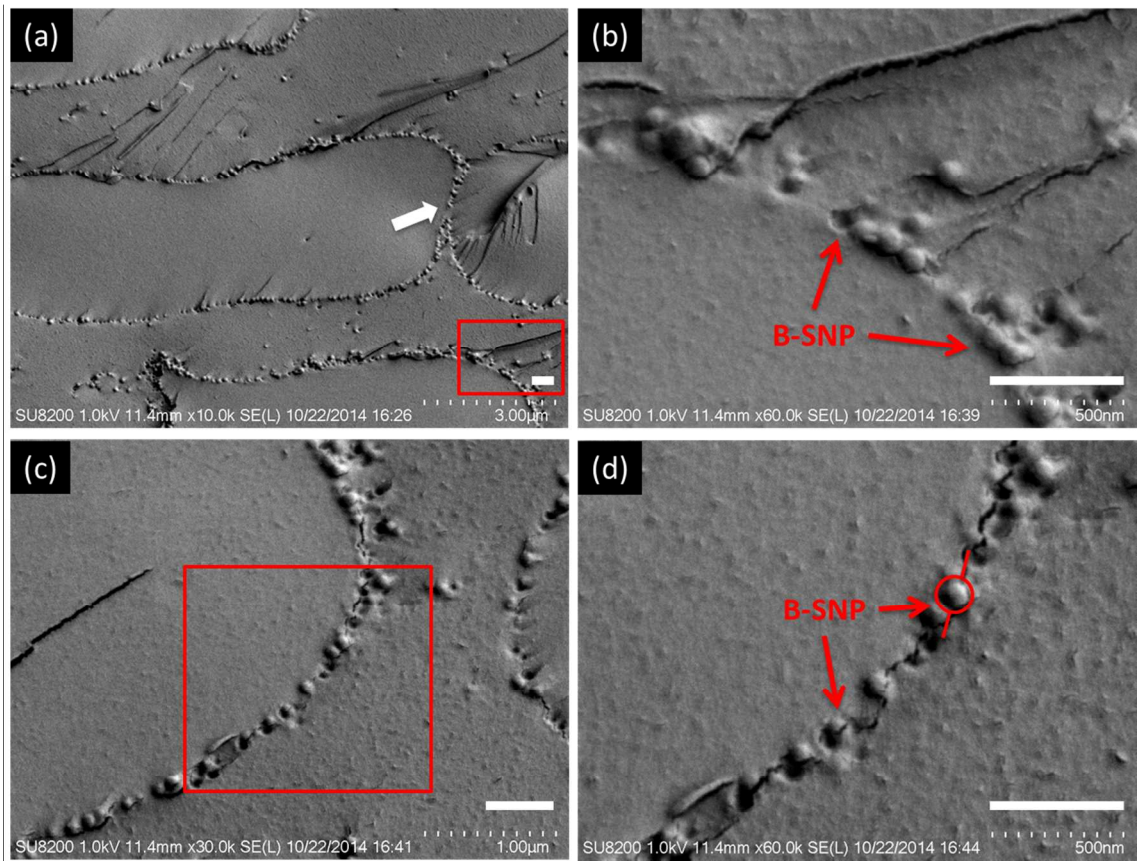

Fig. 5 Cryo-SEM images of the PS/PB/B-SNP (50/50/4.5) bijel. (b) and (d) are magnified views of the rectangular regions indicated in (a) and (c). The white arrow indicates particles straddling or bridging two domains. The red arrows mark individual silica particles or a crater formed by one. The lines on the circled

particle are through the cracks on each side of the particle, which likely run through the interface. The scale bar is 500 nm.

Trapping hydrophobic particles at the interface can be easily understood from a thermodynamic perspective. According to Young's equation,[17,33] the wettability coefficient ω is defined as,

$$\omega = \cos\theta = (\gamma_{\text{Si-PS}} - \gamma_{\text{Si-PB}}) / \gamma_{\text{PS-PB}} \quad (1)$$

where θ is the particle contact angle at the interface (Fig. 6), $\gamma_{\text{PS-PB}}$ is interfacial tension between PS and PB, and $\gamma_{\text{Si-PB}}$ and $\gamma_{\text{Si-PS}}$ are the interfacial tensions between the particle and PB and PS, respectively. The criterion for locating particles at the interface is $-1 < \omega < 1$ ($0^o < \theta < 180^o$). Particles are located in the PB phase when $\omega > 1$ and in the PS phase when $\omega < -1$. We used the Owens-Wendt-Rabel-Kaelble (WORK) approximation to estimate the interfacial energies.[34,35]

$$\gamma_{\text{PS-PB}} = \gamma_{\text{PS}} + \gamma_{\text{PB}} - 2\sqrt{\gamma_{PS}^{d}\gamma_{PB}^{d}} - 2\sqrt{\gamma_{PS}^{p}\gamma_{PB}^{p}} \quad (2)$$

where γ_i^d and γ_i^p are the dispersive and polar parts of the surface tension of component i in the system, which are available in the literature for PB, PS, P-SNP and B-SNP (Table 2).[33,34] From Eq. (1) and (2), the wetting coefficients for PS/PB/P-SNP and PS/PB/B-SNP blends are −4.65 and 0.12, respectively. These results agree with the experimental observation in Fig. 4, i.e., P-SNP aggregate in the PS phase while B-SNP locate at the interface. Moreover, from the cryo-SEM results we estimate, very roughly, the contact angle at ~ 90^o for the B-SNP on the interface of PS and PB (e.g the circled particle in Fig. 5d) which agrees well with the predicted value of 83.1^o calculated from Eq. (1). Hence, our experiments and theoretical analysis demonstrate that capillary forces are sufficient to trap particles of appropriate wetting properties at the interface and form monolayers. The electrostatic repulsion prevailing in polar systems is not a necessary condition for creating nonpolar bijels.

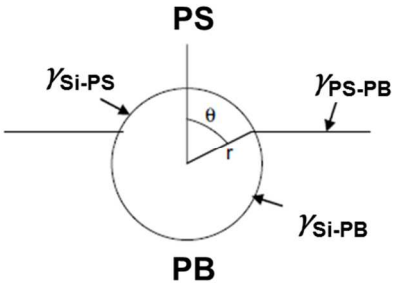

Fig. 6 Schematic of a spherical silica nanoparticle at the interface between PS and PB.

Table 2 Surface tensions and wetting coefficients of the blends

System	Interfacial tension (mN/m)*		ω	Particles location
	PS / PB	6.21		
PS / PB /P-SNP	PS / P-SNP	21.67	−4.65	PS phase
	PB / P-SNP	50.74		
	PS/PB	6.21		
PS / PB /B-SNP	PS / B-SNP	1.37	0.12	interface
	PB / B-SNP	2.10		

* The surface tensions of each component are (in mN/m): γ_{PS} = 40.7 (γ_{PS}^{d} = 34.5, γ_{PS}^{p} = 6.1), γ_{PB} = 33.6 (γ_{PB}^{d} = 33.6, γ_{PB}^{p} = 0), $\gamma_{P\text{-}SNP}$ =80.0 (γ_{P-SNP}^{d} = 29.4, γ_{P-SNP}^{p} = 50.6), $\gamma_{B\text{-}SNP}$ =32.0 (γ_{B-SNP}^{d} = 30.0, γ_{B-SNP}^{p} = 2.0).[33,34]

3.2 Dynamics of coarsening

Fig. 7a shows the characteristic domain size (ξ) plotted against annealing time at room temperature for both the neat blend and PS/PB/B-SNP bijel with different particle loadings (Supplementary Video SV2 – S5). As can be seen from the inset of Fig. 7a, the neat blend shows a continuous increase in domain size. The change of morphology for the neat blend is shown in Fig. 8a and Video SV2 in the Supplementary Information, which displays the change from an initial bicontinuous structure with small domain size to a final drop-matrix structure.

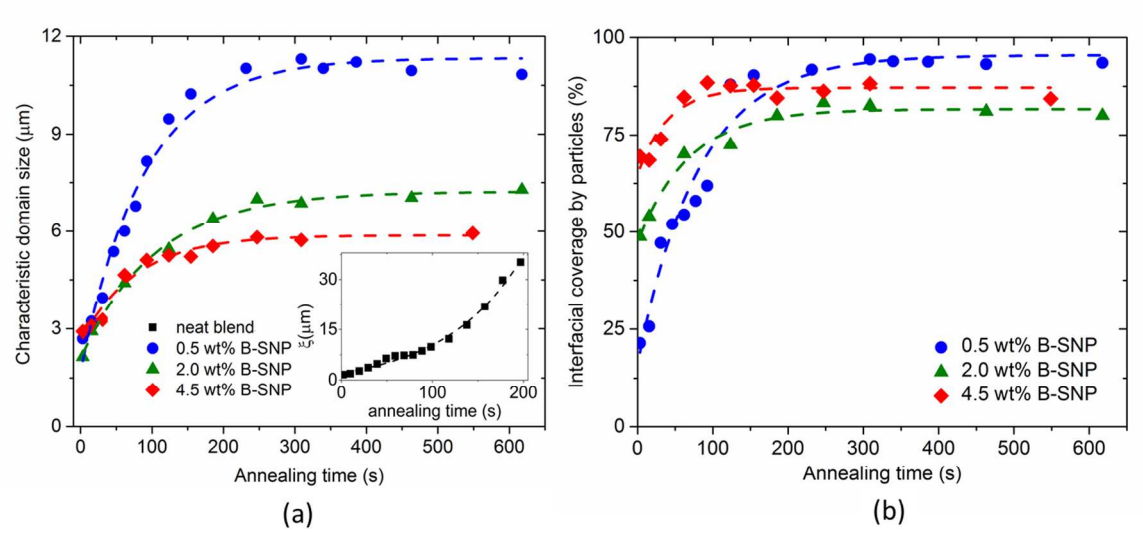

Fig. 7 (a) Characteristic domain size (ξ) as a function of annealing time for PS/PB neat blend (inset) and PS/PB/B-SNP bijels with different weight fraction of particles at 20 ^{o}C ; (b) Interfacial particle coverage as a function of annealing time for PS/PB/B-SNP bijels with different weight fraction of particles at 20 ^{o}C. The dashed lines in both figures are exponential fits (Table 3).

In contrast, the characteristic domain size of the PS/PB/B-SNP (50/50/0.5) bijel increases initially then plateaus at later times (Fig. 7a). With low particle concentration (0.5 wt%) the bicontinuous structure is stabilized with a large domain size (Fig. 8b and Video SV3 in the Supplementary Information). Similar trends were observed when the weight fraction of particles is increased to 2.0 wt% and 4.5wt% (Fig. 7a). In these cases, the bicontinuous morphology changes much less during annealing and stabilizes at a smaller domain size (Fig. 8c and Video SV4 and SV5 in the Supplementary Information), indicating that coarsening of the bicontinuous morphology is more effectively suppressed.

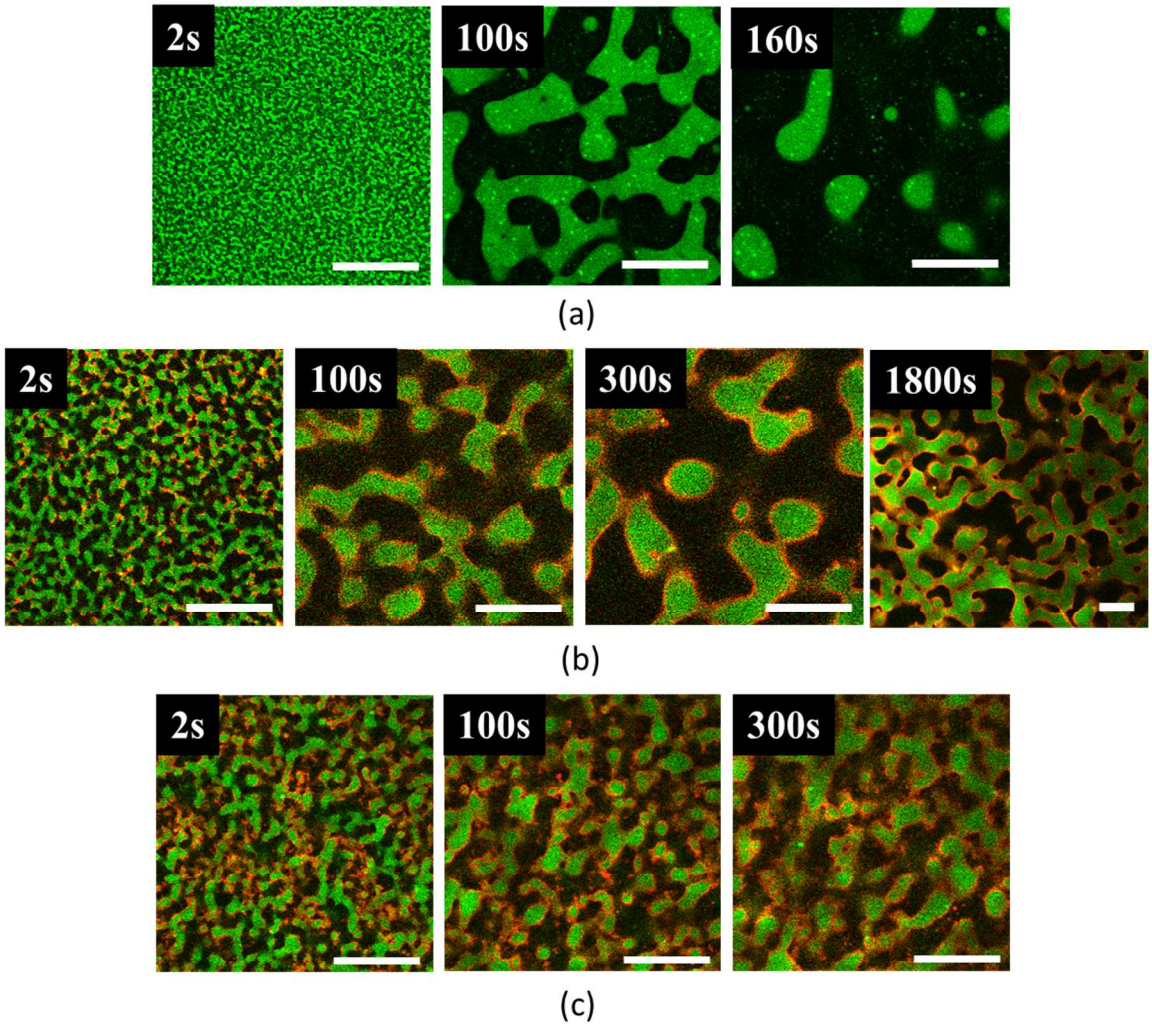

Fig. 8 Confocal images from real-time observation of (a) PS/PB neat blend, (b) PS/PB/B-SNP (50/50/0.5) bijel and (c) PS/PB/B-SNP (50/50/4.5) bijel. The scale bar is 40 μm. Note that the scale bar in the last image of (b) is significantly smaller than others.

Although previous studies on polar bijels have qualitatively shown the change of morphology during coarsening using confocal microscopy[5,9], the increase of interfacial particle coverage has not been quantitatively analyzed. Here, to unambiguously demonstrate the effect of particles in stabilizing the bicontinuous structure, we quantify interfacial particle coverage (SNP %) using the algorithm described in Sec. 2.4. Fig. 7b shows SNP% as a function of annealing time. The B-SNP (red dots in Fig. 8b and 8c when t = 2 s) are sparsely distributed on the interface of the blends at the beginning of annealing. The initial coverage depends on initial particle concentration (Fig. 7b). As the

interfacial area shrinks with annealing, coverage increases. The correlation between the morphology of the blends and interfacial particle coverage is most pronounced when comparing Fig. 7a and 7b: the increase of interfacial coverage is accompanied by a slow-down of coarsening. Interfacial particle coverage reaches a plateau around the time when domain size also reaches a constant. The plateau value in interfacial coverage is approximately the same for all three initial particle concentrations, but slightly smaller than 100%, presumably due to the finite resolution and pixel noises of our imaging.

Cheng and Velankar[15] showed that interfacial particles collect into patches on interfaces of nonpolar drops. Fig. 9 demonstrates that patches form on our nonpolar bijels. In the early stage of coarsening (t = 30s and 60s), particles cannot fully cover the interface and form patches because of the existence of capillary forces between neighboring particles. However, in polar bijels, particles sparsely distribute on the interface rather than form patches because electrostatic repulsion (Coulomb or dipole-dipole interaction) can balance capillary attraction[5,15,37]. In the late stage of coarsening (t = 150s and 300s), neighboring patches merge together with the shrinkage of interfacial area and form the fully covered monolayer of interfacial particles shown in the cryo-SEM images (Fig. 5). It is worth noting that the diameter of SNP used in the experiment (~100 nm) is smaller than the size of each pixel (~330 nm) in the binary images which is limited by the resolution of optical microscopy.

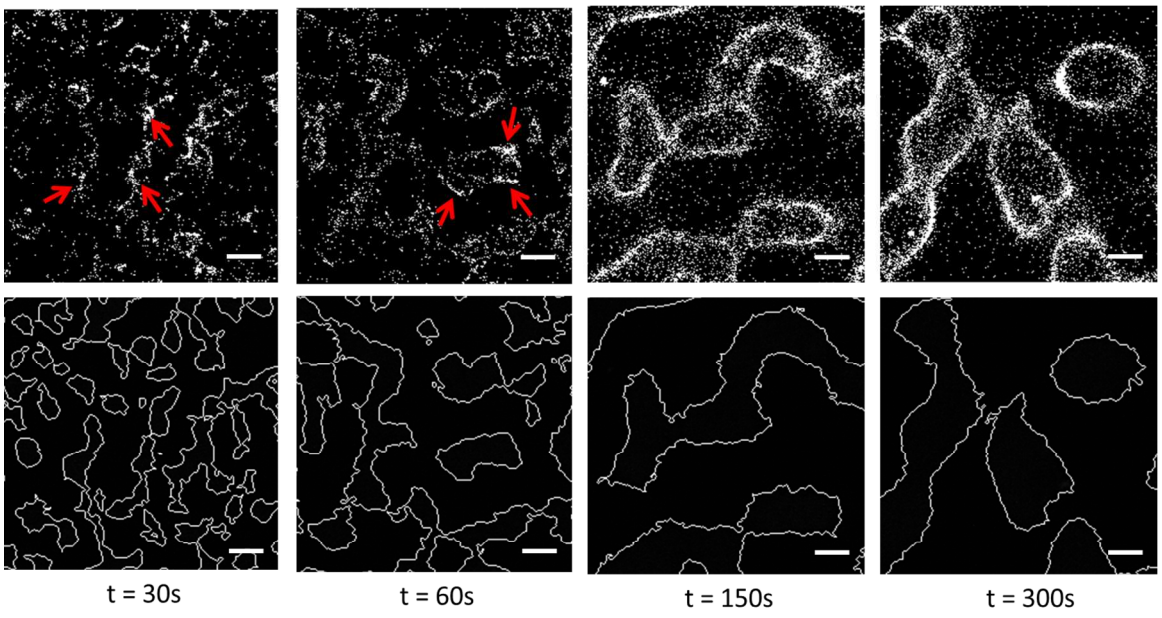

Fig. 9 Binary confocal images of the PS/PB/B-SNP (50/50/0.5) bijel during coarsening. Red arrows mark "patches", localized regions of high particle concentration in the interface, which merge into fully covered interfaces during coarsening. Images in the first row were created using the 563 nm laser which reflects the location of SNP. Images in the second row were derived by tracing the perimeters of the fluorescent PS domains with 488 nm laser. The scale bar is 10 μm.

To quantitatively correlate the change of morphology and particle configurations in bijels, we fit the dynamics of domain size (ξ) and interfacial particle coverage (SNP %) with a simple exponential function:

$$y = y_0 + Ae^{-(t-t_0)/\tau} \quad (3)$$

where y can be ξ or SNP %, y_0 is their plateau value. A, t_0 and τ are fitting parameters where τ is the relaxation time of the process. As shown in Table 3, the domain size and the interfacial particle coverage show similar relaxation times illustrating the direct correlation between interfacial coverage and stabilization of bicontinuous morphology. Furthermore, the results also show that a higher particle concentration leads to a faster suppression of the coarsening.

Table 3 Characteristic times from exponential fitting of characteristic domains size, interfacial coverage by particles and G'

	Characteristic time (s)		
PS/PB/B-SNP bijel (50/50/x)	**from domain size (τ in Eq. 3)**	**from interfacial coverage (τ in Eq. 3)**	**from *G'* time sweep (minimum values of *G'*)**
0.5 wt%	89.2 ± 9.2	81.5 ± 11.3	143.5 ± 15.0
2.0 wt%	105.1 ± 9.8	67.5 ± 13.2	104.0 ± 15.0
4.5 wt%	76.8 ± 13.6	39.8 ± 14.1	26.0 ± 15.0

When particles cover the interface (plateau in Fig. 7b), they suppress and even prohibit coarsening in three possible ways. First, interfacial particles increase the rigidity of the bicontinuous interface. The increase in rigidity decreases deformability of the interface, thus retarding shrinkage of interfacial area. When the interface is full of particles, it cannot further shrink and coarsening of the interface stops (morphology changes in Fig. 8b and Fig. 8c). Second, "interfacial jamming" — a mechanism that also prevents the coalescence of Pickering emulsions[35,38]— enables the particles form a solid barrier at the interface which provides steric hindrance to the coalescence of contacting domains from the same phase. Third, "particle-bridging"[39,40,41,42], which means a monolayer of particles simultaneously bridges across two domains from the same phase to prevent their coalescence, is also responsible for stabilization of bicontinuous morphology (white arrow in Fig. 5a). The first mechanism clearly provides the main contribution to morphology stabilization. As seen in Figures 4b, 5 and 9 most of the particles on the interface neither form a steric barrier to induce "interfacial jamming" nor are they adsorbed across two interfaces to induce "particle-bridging". On the other hand, at the cessation of coarsening full coverage of particles on the interface can be observed throughout the system. Quantitatively, the correlation between the stabilization of the morphology and the change of interfacial particle coverage in Fig. 7 also provides strong support to the first mechanism.

3.3 Rheology of PS/PB/B-SNP bijels

While confocal microscopy illustrates the dynamics of morphology change during coarsening, rheological measurement allows us to explore the influence of morphology on the mechanical properties of the nonpolar bijel. We measured the storage (G') and loss (G'') moduli of PS/PB/B-SNP bijels during coarsening at room temperature and correlated the rheology with the dynamics of bicontinuous structure from confocal imaging. Three different mechanisms contribute to the storage modulus (G') of PS/PB/B-SNP bijels: elasticity of the PS and PB components (G'_{comp}), capillary restoration due to bending of the bare interfaces (G'_{int}) and the particle network at the interface (G'_{SNP}).[43] Since G'_{comp} from the PS and PB components are small (~ 0.1-1Pa), we can safely neglect its contribution. Therefore, $G' \approx G'_{int} + G'_{SNP}$.

The time evolution of G' of PS/PB neat blend and PS/PB/B-SNP bijels during annealing at room temperature is shown in Fig. 10. The rheological behavior of PS/PB (50/50 wt%) neat blend during the time sweep is similar to many bicontinuous polymer blends during annealing[43,44], namely, an apparent initial decrease of G' followed by a gradual decay with slow rate to reach a plateau at long times. The decrease of elasticity is due to the shrinkage of interfacial area with reducing curvature and finally the breakup of the bicontinuous structure into droplets.

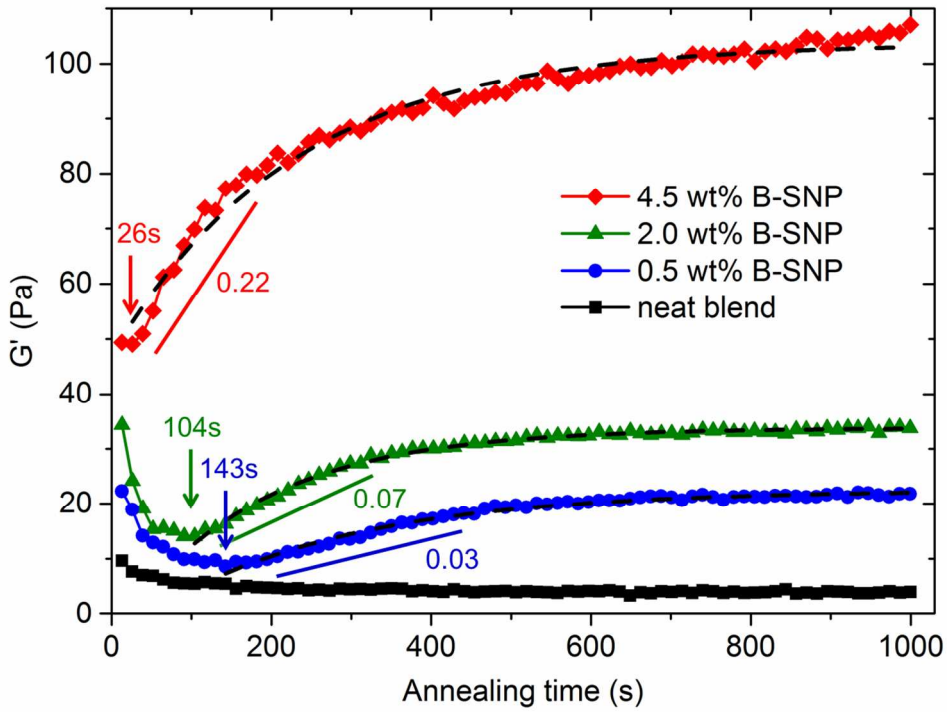

Fig. 10 Storage moduli (*G'*) as a function of annealing time for PS/PB (50/50 wt%) neat blend and PS/PB/B-SNP bijels with different particle loadings. All data were measured at 20 °C, 1 rad/s and 0.1% strain. The dashed lines are exponential fits. The times for the minimum values of *G*' and the rate of increase in G' with annealing time are also indicated.

The rheological behavior of PS/PB/B-SNP bijels is quite different from that of the neat blend: a rapid *G*' decrease in the beginning is followed by a large increase, which eventually plateaus with a plateau value much larger than that of the neat blend. The variation of *G*' with annealing time directly reflects the underlying structural changes in the blend and can be qualitatively understood based on the competition between two opposite structure-induced rheological changes. As shown in Fig. 7 and Fig. 8, during coarsening, interfacial area shrinks with the increase of domain size, leading to the decrease of G'_{int}. Meanwhile, particle patches form and grow, stiffening the interface, resulting in an increase of G'_{SNP}. For the PS/PB/B-SNP (50/50/4.5) bijel, the minimum of *G*' occurs at 26 s followed by a steep increase (slope = 0.22 Pa/s). When particle loading is reduced, the minimum of *G*' appears at a later time (104 s for 2.0 wt% B-SNP and 143 s for 0.5 wt% B-SNP). The increase of *G'* also becomes much slower (slope = 0.07 Pa/s for 2.0 wt% B-SNP and 0.03 Pa/s for 0.5 wt% B-SNP). Therefore, the effect of G'_{SNP}

gradually decreases with the decrease of particle loading. The annealing time at the minimal *G'* characterizes the structural change of bicontinuous phases, which qualitatively matches the time scale measured from direct imaging (Table 3). In addition, blends with higher particle loading and smaller domain size also have larger elastic modulus (*G*' plateau value in Fig. 10). Similar results were also observed in the polar bijels[5,8,18].

After the morphology stabilized the elastic moduli were measured as a function of frequency. Fig. 11 shows, as does Fig. 10, that $G'_{int} >> G'_{SNP}$ over the entire frequency range. The power-law relation of *G*' at low frequencies (ω < 1 rad/s) and the fact that these terminal slopes are much smaller than 2 are rheological signatures of bicontinuous blends[43,44,45].

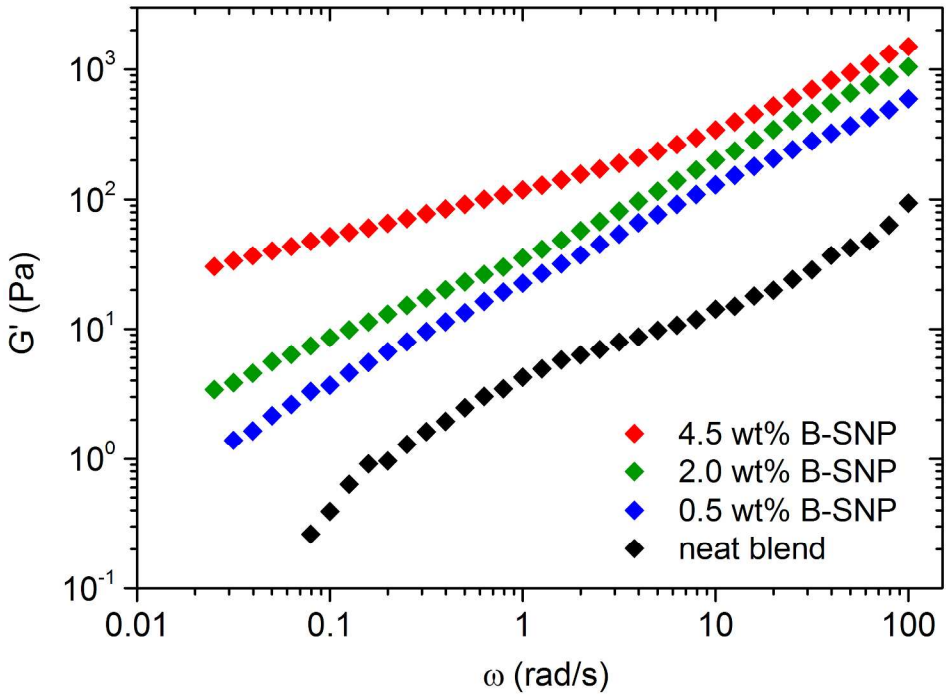

Fig. 11 Dynamic elastic moduli (*G*') as a function of frequency for PS/PB/B-SNP bijels with different weight fractions of B-SNP. All data were measured after 10000 s stabilization from low to high frequency at 20°C and 0.1 % strain.

Comparing the morphology change in Fig. 7a and the rheology response in Fig. 10, we found a surprising effect: *G'* for all three PS/PB/B-SNP bijels continues to increase at

long time scales. For blends with different particle loadings, the bicontinuous structure has already been stabilized by B-SNP after ~ 250 – 300 s (onset of plateau in Fig. 7a). However, *G*' in the blends with 0.5 wt% and 2.0 wt% B-SNP slowly increases and plateau ~500 s. For the PS/PB/B-SNP (50/50/4.5) bijel, the plateau of *G*' was not reached within our measurement window (> 1000 s). A similar trend with a slow continuous increasing of *G'* during annealing has also been observed in polar bijel systems[18], although the effect was not explicitly mentioned or discussed in the paper. Moreover, our preliminary results on bicontinuous blends of immiscible polymers (low density polyethylene/polyethylene oxide) stabilized by interfacial silica nanoparticles also show a qualitatively similar trend[19]. Hence, the slow increase of *G'* at long times seems to be a feature of many particle-stabilized bicontinuous materials.

We hypothesize that the continuous increasing of *G*' arises from intrinsic slow particle rearrangement along the interface of bicontinuous structure long after the morphology has been stabilized. The rearrangement leads to denser particle packing on the interface and thus larger *G*'. Due to the small size of B-SNP (~100 nm) and the resolution limit of confocal microscopy, the rearrangement of particles at the interface cannot be directly observed. However, such rearrangement can be picked up by indirect yet more sensitive rheological measurements. In addition, the observation that higher particle loading leads to slower increase of *G'* can also be explained by this hypothesis. Indeed, it has been shown that a larger spatial curvature leads to more frustrated particle packing and, therefore, slower particle dynamics in the glassy state.[46] Hence, the smaller pore size and the higher interfacial curvature in the PS/PB/B-SNP (50/50/4.5) bijel more effectively slow down the particle rearrangement and thus lead to a very slow increasing in *G'* even after 1000 s annealing (Fig. 10 and Fig. 11).

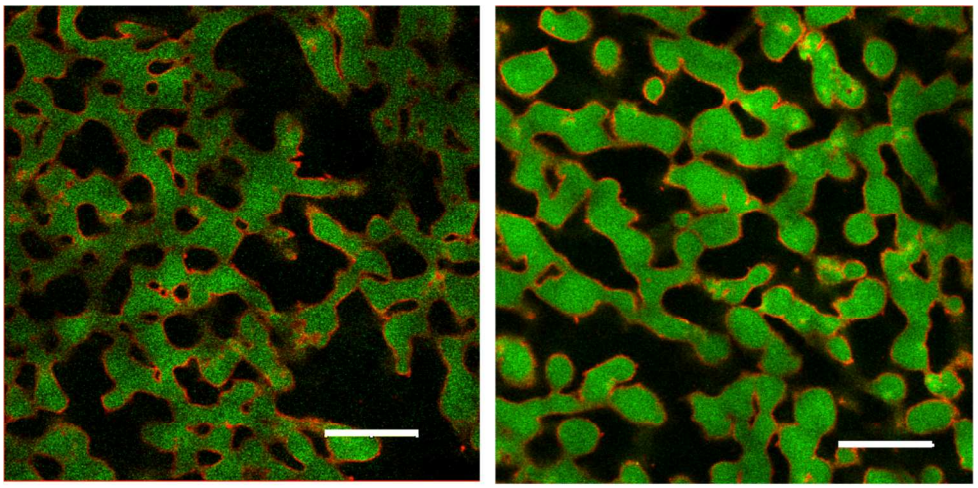

Fig. 12 Confocal images of the PS/PB/B-SNP (50/50/4.5) bijel: (a) after annealing for 15min without shear (b) after annealing for 15min with shear at 1 rad/s, 0.1% strain. The scale bar is 40 μm.

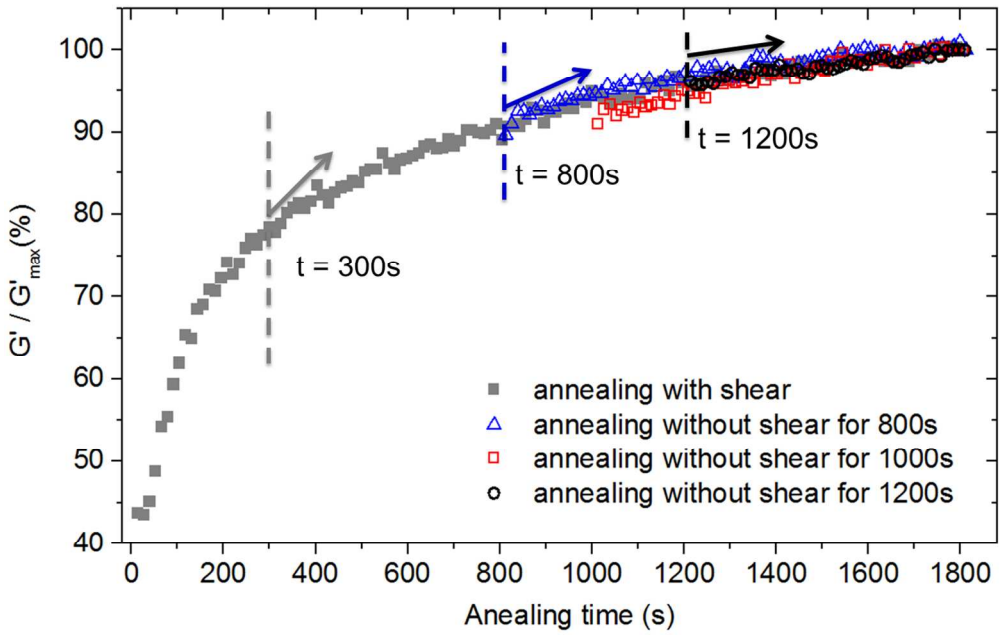

Fig. 13 Storage moduli (*G'*) as a function of annealing time for PS/PB/B-SNP (50/50/4.5) bijels with different pre-annealing time without shear. All data were measured at 20 °C, 1 rad/s and 0.1 % strain. The slopes at different annealing time are illustrated by the arrows in the plot.

We do not believe that the slow increase in *G'* is due to shearing the sample or to inhomogeneity. Fig. 12 shows the same morphology is observed after 15 min of annealing with or without shear. Fig. 13 demonstrates that the increase in *G'* is independent of when the shear was started. Since most of the confocal images were

collected within ~30 μm of the glass cover slip, one might argue that the rheology of the bulk sample could differ. However, Fig. 12b was taken from the fracture of a rheology sample which was 400 μm thick and Fig. 5 is also from a fractured sample. In addition, the gap size between the two parallel plates (400 μm) is much larger than the domain size of bicontinuous blends (~ 10 μm from Fig. 7a). Moreover, this gap size is larger than all other previous bijels with rheology.[8,9] Therefore, we can safely ignore the boundary effect on the rheological measurement.

In summary, we found a new surprising rheological feature of bijels, which seems to be a universal signature of many bicontinuous blends. A hypothesis of slow particle rearrangement along highly-curved bicontinuous interfaces has been proposed. We will explore the possibility to direct image the particle arrangement along the interface at long time scales using larger colloidal particles in future work.

3.4 Formation of monogel

Finally, we also observed the formation of monogel in our nonpolar system. When PS/PB/B-SNP bijels are reheated from room temperature back to 80 ^{o}C, PS and PB remix into a single liquid phase. However, the jammed particle monolayer still remains intact where the interface existed before remixing (Fig. 14a). Because the particle framework comprises a web of locally planar particle monolayers, this “skeleton” structure has been called a “monogel” by Cates *et al*.[20]

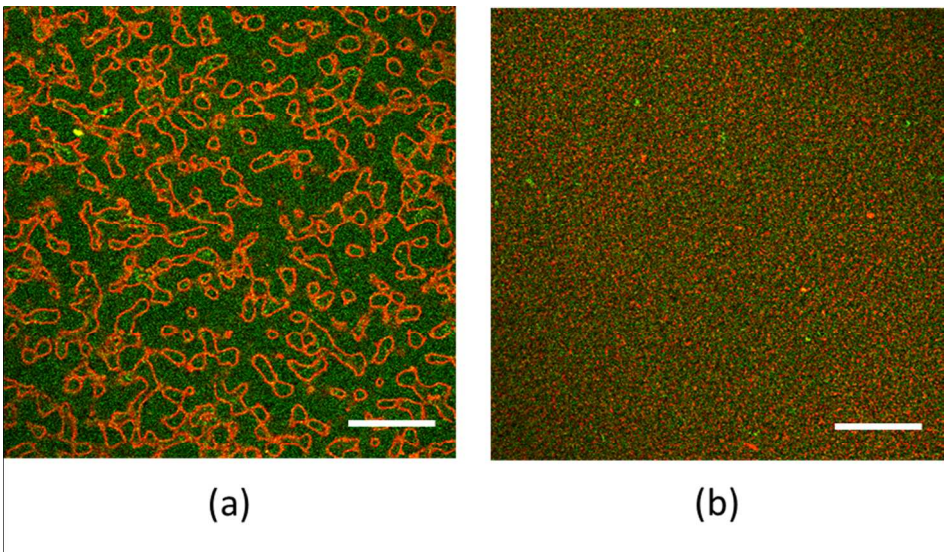

Fig. 14 Confocal images of the monogel from the PS/PB/B-SNP (50/50/4.5) bijel at 80 ^{o}C: (a) before shear; (b) after shear. The green region is the remixed single-phase matrix, and the red dots represent the hydrophobic particles. The scale bar is 40 μm.

Monogel has been observed in polar bijels composed of water and 2,6-lutidine (water/oil)[18,20], where the formation of monogel has been attributed to the stabilization of particles in the primary minimum of the DLVO (Derjaguin-Landau-Verweg-Overbeek) potential[47]. Attractive capillary forces in the water/oil systems overcome electrostatic repulsion and drive particles across the energy barrier of the DLVO potential into the primary van der Waals minimum. In the water/oil systems, short-ranged attraction stems from the van der Waals force between particles while long-ranged repulsion is due to the weak, negative electrostatic charge of the dissociated silanol groups on the surface of hydrophilic particles (P-SNP).[20,48] When B-SNP were used to stabilize the polar bijels (e.g. bijel of nitromethane and ethylene glycol), the HMDS graft layers on B-SNP hindered the formation of monogel.[8] This is due to the solvation of HMDS layers by the dissociated nitromethane molecules, which enhances the negative electrostatic charges on the particles, thus breaking the balance between long-range repulsion and short-range attraction and impeding the rearrangement of B-SNP.[8] However, in our nonpolar PS/PB/B-SNP bijels, both PS and PB molecules are hardly dissociated and thus do not solvate the HMDS graft layers. It is highly possible that the particles in the nonpolar

blend experience a smaller repulsive barrier compared with that of polar blends and are easily driven to the primary minimum by capillary attractions. Therefore, the nonpolar nature of the PS and PB facilitates the formation of monogel with B-SNP.

To test the strength of the B-SNP monogel, it was sheared sinusoidally at increasing strain amplitude (Fig. 15). In the first strain sweep, the monogel displays signatures of gel-like rheology, G' and G" are constant at small γ and G_o' > G_o". The crossover of G' and G" at strain of around 1.0 %, is often regarded as the onset of yielding of a solid-like structure. This rheological behavior under a strain sweep is also observed in many colloidal gel systems.[49,50,51] However, G_o' decreased by an order of magnitude after the shear from the first sweep. The great decrease in G_o' can be explained by the morphology change of the B-SNP monogel under shear. The particle network is completely destroyed by shear and collapses into clusters of particles dispersed in the single phase matrix (Fig. 14b). Without the process of spinodal decomposition serving as a template to guide particles, the dispersed particles cannot re-aggregate in the form of locally planar monolayers. Therefore, the breakup of the particle network is irreversible.

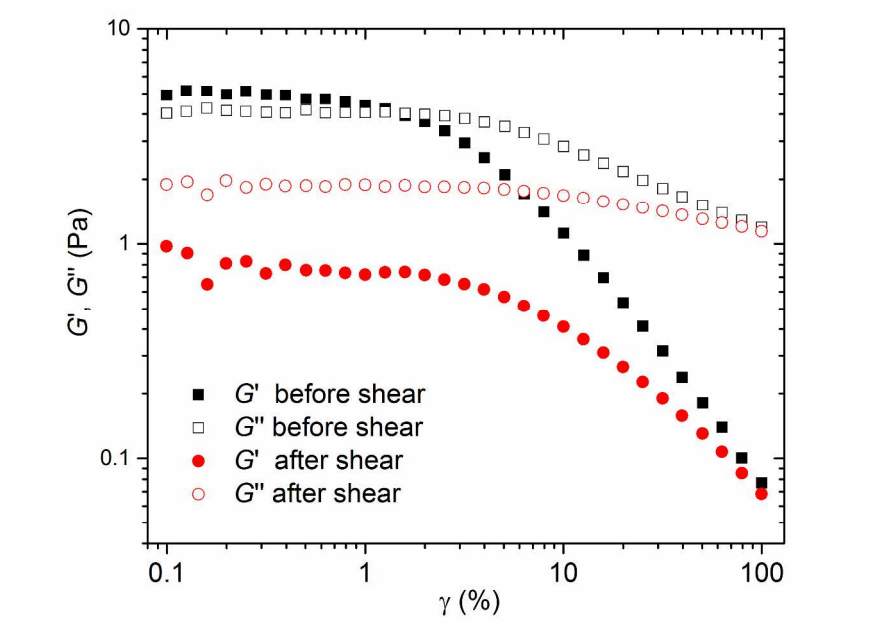

Fig. 15 The storage (G') and loss (G") moduli of the monogel as a function of sinusoidal shear strain amplitude (γ). All data were measured at 80°C with a frequency of 1 rad/s.

4. Conclusions

We have developed a nonpolar bijel composed of styrene trimers (PS) and low molecular weight polybutene (PB) that is stabilized by a monolayer of hydrophobic silica nanoparticles (B-SNP) at the interface. We have studied the mechanism by which interfacial silica nanoparticles suppress coarsening in nonpolar bijels. Interfacial localization of B-SNP was demonstrated using confocal microscopy, and the monolayer structure was further confirmed by high magnification cryo-SEM. Real-time dynamics of coarsening with different particle loadings were investigated via multi-channel confocal microscopy. We have developed a new algorithm to calculate the change of interfacial particle coverage with annealing time, and unambiguously demonstrated that interfacial particle coverage is the leading factor for the suppression of coarsening and stabilization of bicontinuous structure. We also observed that interfacial particles cluster into patches, which merge during coarsening in our nonpolar bijels. This phenomenon has not been observed in the polar bijels.

In addition, we quantitatively correlate morphology and interfacial particle coverage with rheology measurements. Competition between the shrinkage of interface and the formation of a particle network results in a non-monotonic rheological response of PS/PB/B-SNP bijels in the early annealing stage. We also uncovered a slow increase of the storage modulus after the stabilization of bicontinuous morphology, which we argue is a feature of many bicontinuous blends. By eliminating alternatives, we suggest that such a surprising phenomenon is due to the intrinsic slow particle rearrangement on the curved interface. One possible direction for future research is to employ a newly-designed confocal rheoscope to simultaneously measure rheology, morphology change and particle rearrangement using micron-size colloidal particles in bicontinuous blends[52]. Finally, thanks to the nonpolar nature of the PS/PB/B-SNP system, we observed the formation of monogel by hydrophobic particles. Moreover, the irreversibility of the

monogel derived from nonpolar blends under shear was also demonstrated.

Compared with low-viscosity polar bijels, the styrene trimers and polybutenes used in our study are more relevant to polymer blends that have even greater potential for technical applications[35]. As such, our study on the PS/PB/B-SNP bijels also opens a door for probing the correlation between the dynamics and the rheology of bicontinuous polymer blends[19].

5. Acknowledgement

The authors are grateful to Dr. Garrett Swindlehurst for his help in the synthesis of the fluorescent silica nanoparticles, Dr. Guillermo Marques and Dr. John Oja of University Imaging Centers for their help in image acquisition, Dr. Aaron Hedegaard and Miss Yalin Liu for their help in image processing and analysis, Mr. Chris Frethem for his help in cryo-SEM and reviewers for helpful suggestions. The authors thank the members of the University of Minnesota Industrial Partnership for Research in Interfacial and Materials Engineering (IPRIME) for financial support and the Undergraduate Research Opportunities Program (UROP) from University of Minnesota for its financial support to John W. Fruehwirth.

References

1. K. Stratford, R. Adhikari, I. Pagonabarraga, J.-C. Desplat, and M. E. Cates, *Science*, 2005, **309**, 2198–2201.

2. M. E. Cates and P. S. Clegg, *Soft Matter*, 2008, **4**, 2132–2138.

3. S. G. Lévesque, R. M. Lim, and M. S. Shoichet, *Biomaterials*, 2005, **26**, 7436–46.

4. M. Martina, G. Subramanyam, J. C. Weaver, D. W. Hutmacher, D. E. Morse, and S. Valiyaveettil, *Biomaterials*, 2005, **26**, 5609–16.

5. E. M. Herzig, K. A. White, A. B. Schofield, W. C. K. Poon, and P. S. Clegg, *Nat. Mater.*, 2007, **6**, 966–971.

6. J. R. Wilson, W. Kobsiriphat, R. Mendoza, H.-Y. Chen, J. M. Hiller, D. J. Miller, K. Thornton, P. W. Voorhees, S. B. Adler, and S. A. Barnett, *Nat. Mater.*, 2006, **5**, 541–4.

7. M. N. Lee and A. Mohraz, *Adv. Mater.*, 2010, **22**, 4836–4841.

8. J. W. Tavacoli, J. H. J. Thijssen, A. B. Schofield, and P. S. Clegg, *Adv. Funct. Mater.*, 2011, **21**, 2020–2027.

9. J. A. Witt, D. R. Mumm, and A. Mohraz, *Soft Matter*, 2013, **9**, 6773 – 6780.

10. L. Botto, E. P. Lewandowski, M. Cavallaro, and K. J. Stebe, *Soft Matter*, 2012, **8**, 9957.

11. L. Botto, L. Yao, R. L. Leheny, and K. J. Stebe, *Soft Matter*, 2012, **8**, 4971.

12. L. Yao, L. Botto, M. Cavallaro, Jr, B. J. Bleier, V. Garbin, and K. J. Stebe, *Soft Matter*, 2013, **9**, 779–786.

13. M. G. Nikoladies, A. R. Bausch, M. F. Hsu, A. D. Dinsmore, M. P. Brenner, C. Gay, and D. A. Weitz, *Nature*, 2002, **420**, 299–301.

14. K. Masschaele, B. J. Park, E. M. Furst, J. Fransaer, and J. Vermant, *Phys. Rev. Lett.*, 2010, **105**, 048303.

15. H.-L. Cheng and S. S. Velankar, *Langmuir*, 2009, **25**, 4412–20.

16. J. Vermant, G. Cioccolo, K. Golapan Nair, and P. Moldenaers, *Rheol. Acta*, 2004, **43**, 529–538.

17. S. Vandebril, J. Vermant, and P. Moldenaers, *Soft Matter*, 2010, **6**, 3353–3362.

18. M. N. Lee, J. H. J. Thijssen, J. A. Witt, P. S. Clegg, and A. Mohraz, *Adv. Funct. Mater.*, 2013, **23**, 417–423.

19. S. Huang, L. Bai, M. Trifkovic, X. Cheng, and C. W. Macosko, *manuscript in preparation.*, 2015.

20. E. Sanz, K. A. White, P. S. Clegg, and M. E. Cates, *Phys. Rev. Lett.*, 2009, **103**, 255502.

21. H. J. Chung, K. Ohno, T. Fukuda, and R. J. Composto, *Nano Lett.*, 2005, **5**, 1878–1882.

22. S. Gam, A. Corlu, H.-J. Chung, K. Ohno, M. J. a. Hore, and R. J. Composto, *Soft Matter*, 2011, **7**, 7262–7268.

23. H. J. Chung, J. Kim, K. Ohno, and R. J. Composto, *ACS Macro Lett.*, 2012, **1**, 252–256.

24. T. Xia, Y. Huang, X. Jiang, Y. Lv, Q. Yang, and G. Li, *Macromolecules*, 2013, **46**, 8323–8333.

25. A. F. M. Barton, *Handbook of Solubility Parameters and Other Cohension Parameters*, CRC Press, Second Edi., 1991.

26. J. Kressler, H. W. Kammer, and K. Klostermann, *Polym. Bull.*, 1986, **119**, 113–119.

27. W. Stober and A. Fink, *J. Colloid Interface Sci.*, 1968, **69**, 62–69.

28. G. H. Bogush, M. A. Tracy, and C. F. Zukoski, *J. Non. Cryst. Solids*, 1988, **104**, 95–106.

29. M. A. Hillmyer, W. W. Maurer, T. P. Lodge, F. S. Bates, and K. Almdal, *J. Phys. Chem. B*, 1999, **103**, 4814–4824.

30. C. J. Ellison, A. J. Meuler, J. Qin, C. M. Evans, L. M. Wolf, and F. S. Bates, *J. Phys. Chem. B*, 2009, **113**, 3726–3737.

31. A. A. Lefebvre, N. P. Balsara, J. H. Lee, and C. Vaidyanathan, *Macromolecules*, 2002, **35**, 7758–7764.

32. Y. Lipatov, *Prog. Polym. Sci.*, 2002, **27**, 1721–1801.

33. D. W. van Krevelen, *Properties of Polymers 3rd ed.*, Elsevier, 1990.

34. L. Elias, F. Fenouillot, J. C. Majeste, and P. Cassagnau, *Polymer.*, 2007, **48**, 6029–6040.

35. F. Fenouillot, P. Cassagnau, and J.-C. Majesté, *Polymer.*, 2009, **50**, 1333–1350.

36. N. Virgilio, C. Marc-Aurele, and B. D. Favis, *Macromolecular*, 2009, **42**, 3405–3416.

37. P. S. Clegg, E. M. Herzig, A. B. Schofield, S. U. Egelhaaf, T. S. Horozov, B. P. Binks, M. E. Cates, and W. C. K. Poon, *Langmuir*, 2007, **23**, 5984–5994.

38. W. Tong, Y. Huang, C. Liu, X. Chen, Q. Yang, and G. Li, *Colloid Polym. Sci.*, 2010, **288**, 753–760.

39. P. Thareja and S. Velankar, *Rheol. Acta*, 2006, **46**, 405–412.

40. P. Thareja and S. Velankar, *Rheol. Acta*, 2008, **47**, 189–200.

41. S. P. Nagarkar and S. S. Velankar, *Soft Matter*, 2012, **8**, 8464–8477.

42. S. Nagarkar and S. S. Velankar, *J. Rheol.*, 2013, **57**, 901–926.

43. C. R. López-Barrón and C. W. Macosko, *J. Rheol.*, 2012, **56**, 1315–1334.

44. I. Vinckier and H. M. Laun, *Rheol. Acta*, 1999, **38**, 274–286.

45. J. Gao, C. Huang, N. Wang, W. Yu, and C. Zhou, *Polymer*, 2012, **53**, 1772–1782.

46. F. Sausset, G. Tarjus, and P. Viot, *Phys. Rev. Lett.*, 2008, **101**, 155701.

47. J. N. Israelachvili, *Intermolecular and Surface Forces*, Elsevier, 2011.

48. K. A. White, A. Schofield, B, B. P. Binks, and P. S. Clegg, *J. Phys. Condens. Matter*, 2008, **20**, 494223.

49. L. C. Hsiao, R. S. Newman, S. C. Glotzer, and M. J. Solomon, *Proc. Natl. Acad. Sci. U. S. A.*, 2012, **109**, 16029–34.

50. J. Min Kim, A. P. R. Eberle, a. Kate Gurnon, L. Porcar, and N. J. Wagner, *J. Rheol.*, 2014, **58**, 1301–1328.

51. J. Kim, D. Merger, M. Wilhelm, and M. E. Helgeson, *J. Rheol.* , 2014, **58**, 1359–1390.

52. X. Cheng, J. H. McCoy, J. N. Israelachvili, and I. Cohen, *Science*, 2011, **333**, 1276–9.